The EMBO Journal (2008) 27, 2799–2808 | © 2008 European Molecular Biology Organization | Some Rights Reserved 0261-4189/08
www.embojournal.org

THE EMBO JOURNAL

EMBO open

Turning of the receptor-binding domains opens up the murine leukaemia virus Env for membrane fusion

Shang-Rung Wu, Mathilda Sjöberg, Michael Wallin, Birgitta Lindqvist, Maria Ekström, Hans Hebert, Philip JB Koeck and Henrik Garoff*

Department of Biosciences and Nutrition, Karolinska Institute, Huddinge, Sweden

The activity of the membrane fusion protein Env of Moloney mouse leukaemia virus is controlled by isomerization of the disulphide that couples its transmembrane (TM) and surface (SU) subunits. We have arrested Env activation at a stage prior to isomerization by alkylating the active thiol in SU and compared the structure of isomerization-arrested Env with that of native Env. Env trimers of respective form were isolated from solubilized particles by sedimentation and their structures were reconstructed from electron microscopic images of both vitrified and negatively stained samples. We found that the protomeric unit of both trimers formed three protrusions, a top, middle and a lower one. The atomic structure of the receptor-binding domain of SU fitted into the upper protrusion. This was formed similar to a bent finger. Significantly, in native Env the tips of the fingers were directed against each other enclosing a cavity below, whereas they had turned outward in isomerization-arrested Env transforming the cavity into an open well. This might subsequently guide the fusion peptides in extended TM subunits into the target membrane.

The EMBO Journal (2008) **27,** 2799–2808. doi:10.1038/emboj.2008.187; Published online 18 September 2008
Subject Categories: microbiology & pathogens; structural biology
Keywords: cryo-electron microscopy; Env trimers; image processing; isomerization-arrested state; receptor-binding domain

Introduction

Membrane fusion proteins of enveloped viruses such as influenza and retroviruses are trimeric complexes of a peripheral and a transmembrane (TM) subunit pair (Hunter, 1997; Skehel and Wiley, 2000). The peripheral subunit carries the receptor-binding capacity and the TM subunit the fusion activity. According to the prevailing model, the TM subunit is kept in a metastable, inactive conformation in the native fusion protein. Activation occurs through refolding of the TM subunit into a stable form. This involves exposure of a hydrophobic peptide, the fusion peptide, and the insertion of the latter into the target membrane. Subsequently, the TM subunit back-folds so that the fusion peptide and the membrane anchor orient into the same direction. Through these changes, the virus is able to target the cell membrane and approach it for virus–cell membrane fusion. The peripheral subunit controls the fusion activity, so that it does not occur prematurely and so that it follows a productive pathway at the target membrane. This model has been supported mainly by the atomic structures of the native and activated fusion protein of influenza virus and the activated form of several retroviruses (Wilson *et al*, 1981; Bullough *et al*, 1994; Fass *et al*, 1996; Chan *et al*, 1997; Weissenhorn *et al*, 1997; Kobe *et al*, 1999). However, so far there are no atomic structures of the native form of the retrovirus fusion protein, only of isolated peripheral subunit monomers (Fass *et al*, 1997; Kwong *et al*, 1998; Chen *et al*, 2005; Huang *et al*, 2005). Furthermore, there are no structures of the intermediate forms of the membrane fusion proteins that are believed to mediate the viral and cell membrane fusion reaction.

The membrane fusion protein, Env, of Moloney murine leukaemia virus (Mo-MLV) is a trimer of disulphide-linked peripheral (surface; SU) and TM subunits (Forster *et al*, 2005). The SU is composed of an N-terminal receptor-binding domain, RBD, that is linked to a C-terminal domain by a proline-rich segment (Pinter *et al*, 1982; Fass *et al*, 1997; Lavillette *et al*, 1998; Kayman *et al*, 1999). During activation of the Mo-MLV Env, the receptor-bound RBD transmits a signal to the C-terminal SU domain that results in triggering of the TM subunit (Barnett and Cunningham, 2001; Lavillette *et al*, 2001). The signal activates a thiol in a CXXC motif of the C-terminal domain, where the other Cys residue participates in the formation of the intersubunit disulphide (Pinter *et al*, 1997; Wallin *et al*, 2004). The activated thiol will attack the disulphide and cause its isomerization into a disulphide isomer within the motif. This leads to SU displacement and TM refolding. Significantly, the activation process can be arrested at a stage before disulphide isomerization if an alkylator is present (Wallin *et al*, 2004, 2005b). The CXXC thiol will be exposed because of initial changes in the Env structure and alkylated before it can attack the intersubunit disulphide. Thus, the Env will be arrested at an intermediate stage of its conformational transition, which also blocks membrane fusion and infection of the virus. However, this isomerization-arrested state, IAS, can be relieved by external

*Corresponding author. Department of Biosciences and Nutrition, Karolinska Institute, 141 57 Huddinge, Sweden. Tel.: +46 8 6089125; Fax: +46 8 7745538; E-mail: henrik.garoff@ki.se

Received: 30 May 2008; accepted: 26 August 2008; published online: 18 September 2008

reduction of the SU–TM disulphide with DTT. The receptor-induced triggering of Mo-MLV Env is mediated by the release of Ca^{2+} ion(s) from Env (Wallin *et al*, 2004). Apparently Ca^{2+} stabilizes the native structure of Mo-MLV Env. Accordingly, virus-mediated membrane fusion is stimulated by Ca^{2+} depletion, unspecific protein perturbation and possibly by limited Env proteolysis (Wallin *et al*, 2005a; Kumar *et al*, 2007). As a consequence, the virus can also be activated *in vitro*, for instance by Ca^{2+} depletion and arrested at IAS in the presence of an alkylator.

In the present study, we have isolated native and IAS Env trimers and reconstructed their 3D structures by processing electron microscopic (EM) images of both vitrified and negatively stained trimers. The atomic structure of the Mo-RBD was modelled from that of the related Friend (F)-MLV and found to fit well into the upper protrusions of the native and the IAS Env trimers, creating pseudoatomic models of this part of the oligomers (Fass *et al*, 1997). In native Env, the L-shaped RBD enclosed, in an upside-down position, the upper part of a large central cavity. In IAS Env, the RBDs turned into a new position opening up the cavity from above thus forming an open well. We propose that this is, at a subsequent activation step, used by an extended form of the TM subunits to reach the target membrane with their fusion peptides. Furthermore, the relocation of the RBD might create the necessary signal for activating the intersubunit disulphide isomerization that controls membrane fusion.

Results

Isolation of native and IAS Env trimers

Earlier we showed by blue native (BN)–PAGE that IAS Env trimers can be solubilized from Mo-MLV with a TX-100-based lysis buffer containing EDTA and NEM (Sjöberg *et al*, 2008). Therefore, we used BN–PAGE to find out whether native Env trimers can also be released if the lysis is done under non-activating conditions, that is, in the presence of Ca^{2+}. Thus, [^{35}S]Cys-labelled Mo-MLV was lysed in the presence of Ca^{2+} or EDTA and NEM and the samples were analysed by BN–PAGE and non-reducing SDS–PAGE. Before the latter analysis, NEM was also added to the native Env sample. This was done to save its SU–TM complexes from SDS-induced isomerization. The BN–PAGE showed that it was possible to release native Env trimers (MW about 225 kDa) (Figure 1A, lane 1). These migrated slightly faster than the IAS Env trimer, which is known to be a more open structure, accessible for external reagents (Wallin *et al*, 2004, 2006) (Figure 1A, lane 2). Analysis of the IAS Env sample also showed some SU–TM complex dimers and monomers (Sjöberg *et al*, 2008). Of these, the dimers, but not the monomers, were present in the native Env sample. The dimers migrated closely in front of the native trimers (Figure 1A, lane 1). In contrast to the IAS Env, the native Env sample contained some free SU subunits, probably released by spontaneous activation (Wallin *et al*, 2004). In addition, both samples contained internal viral proteins running in the front part of the BN–PAGE. The non-reducing SDS–PAGE showed that most of the Env subunits were covalently linked into SU–TM complexes (MW 75 kDa) in the native Env sample and that virtually all subunits were linked in the IAS Env sample (Figure 1D, lanes 1 and 2). We then investigated whether native and IAS Env trimers, solubilized at respective conditions from [^{35}S]Cys-labelled Mo-MLV, could be isolated by sedimentation in 5–20% (w/w) sucrose gradients containing TX-100 and Ca^{2+}. The gradients were fractionated and samples of each fraction were analysed by BN– and non-reducing SDS–PAGE. The BN–PAGE showed that most of the native SU–TM trimers sedimented to fraction 9 of the gradient, free from

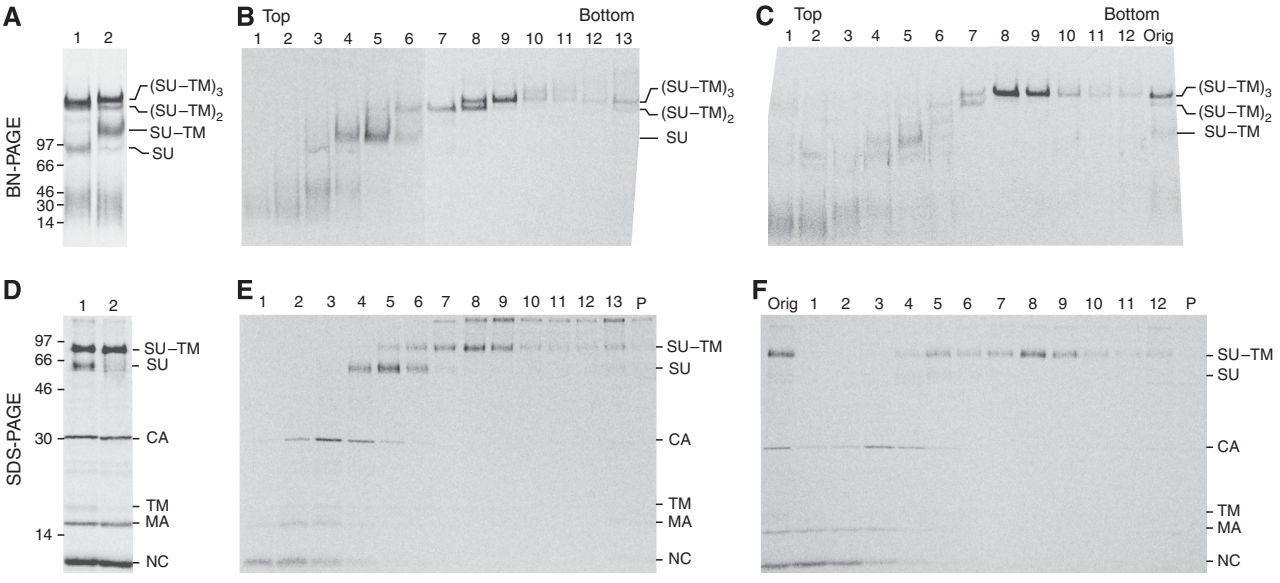

Figure 1 Isolation of native and IAS Env trimers by sedimentation in sucrose gradients. [^{35}S]Cys-labelled Mo-MLV was lysed in HN buffer containing either TX-100 and Ca^{2+} or TX-100, EDTA and NEM to solubilize Env in native state or at IAS. The samples were then subjected to sedimentation in 5–20% (w/w) sucrose gradients. In (**A**), BN–PAGE of the samples with native (lane 1) and IAS Env (lane 2) is shown and in (**D**), the corresponding non-reducing SDS–PAGE is shown. The BN–PAGE of the gradient-fractionated native and IAS Env samples is shown in (**B**, **C**) and the corresponding non-reducing SDS–PAGE is shown in (**E**, **F**). Viral proteins and their state of oligomerization are indicated. Gradient fractions have been numbered from the top. The migration of molecular weight standard proteins is indicated. P, material in pellet; Orig, original sample.

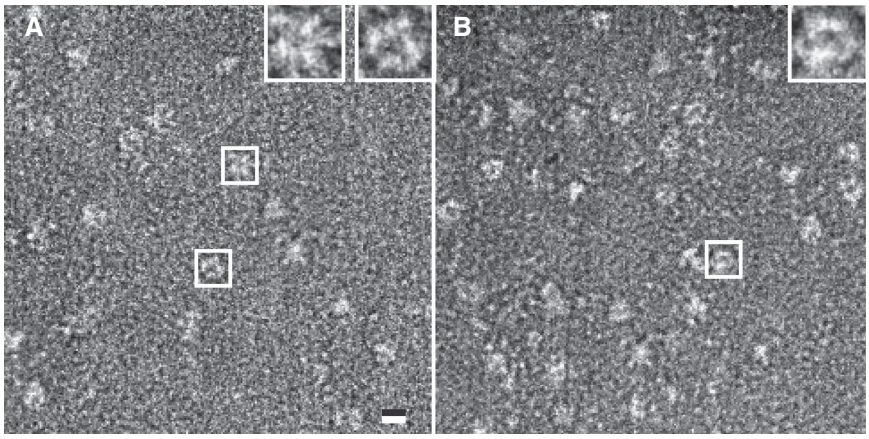

Figure 2 EM analyses of negatively stained native and IAS Env. Sucrose gradient-purified native (**A**) and IAS Env (**B**) were stained with uranyl acetate and subjected to analyses by EM. The boxed images in A (enlarged in inserts) resemble bottom and side views of reconstructed native Env shown in Figures 3 and 4. The boxed image in B resembles a side view of reconstructed IAS Env in Figures 3 and 4. The scale bar represents 10 nm.

other viral proteins (Figure 1B). Trimers and dimers were found in fraction 8 and more dimers in fractions 6 and 7. The SU was seen in fractions 4–6 and smaller proteins in still lighter fractions. The non-reducing SDS–PAGE confirmed the composition of the Env complexes and also identified the smaller viral proteins in the lighter fractions (Figure 1E). Note that some SU–TM complexes were retained at the gel interface in this analysis. Analysis of the IAS Env sample showed that apparently pure IAS Env trimers sedimented to fractions 8 and 9 (Figure 1C and F). We concluded that this procedure is suitable for the isolation of native and IAS Env trimers.

EM of negatively stained native and IAS Env

Purified native and IAS Env trimers in sucrose gradient fractions were applied to EM grids, negatively stained with 2% uranyl acetate and examined by transmission EM. Using both samples, we observed numerous images apparently representing Env molecules fixed in different orientations on the grid (Figure 2A and B). The boxed images of the native sample (magnified in the inserts) resemble bottom and side views of the native reconstructions shown below, whereas the boxed image of the IAS sample is similar to a side view of the IAS reconstructions.

Structures of vitrified and of negatively stained native and IAS Env trimers

The cryo-EM reconstruction of the native Env (7057 particles) showed a trimer of a protomeric unit with three protrusions of different sizes and forms that surrounded a large central cavity (Figure 3, native Env). The trimer had a height along the three-fold axis of 90 Å and a width of 94 Å. The resolution was estimated by Fourier shell correlation to be 19 Å at a correlation coefficient of 0.5. When viewed from the side, that is, perpendicular to the three-fold axis of the trimer, one protrusion (II) of the protomer was in the middle and the two others (I and III) at the ends (Figure 3, native Env, side view 2). The protrusion II was curved in the plane perpendicular to the three-fold axis in a left-handed manner (Figure 3, native Env, top and bottom views). Protrusion I was curved similar to a bent finger towards the three-fold axis in the centre of the oligomer (Figure 3, native Env, side views). Taken together, the three finger-like protrusions limited the central cavity at this end of the Env molecule. We tentatively denote this protrusion the upper (membrane distal) protrusion and the corresponding part of the trimer the Env tip. Thus, the protrusion III at the other end will be denoted the lower (membrane proximal) protrusion. This protruded obliquely outwards and downwards.

The corresponding protomer with three protrusions was also found in the cryo-EM reconstruction of the IAS Env (resolution 19 Å, 6787 particles), but there was a drastic change in the positioning of the protrusion I (Figure 3, IAS Env). The curved finger-like protrusions did not point towards the centre as in native Env, but their tips appeared to have rotated to the periphery so that the upper parts of the protrusions formed a triangular structure around the three-fold axis instead (Figure 3, IAS Env, top view). This change opened up the central cavity of the native Env from above. The positions of protrusions II and III of the IAS Env protomer appeared more similar to those of the native Env. However, the length of protrusion II was reduced and protrusion III appeared slimmer. Additionally, the floor of the cavity appeared thicker in the IAS than in the native form, due to increased density at the three-fold axis (Figure 3, IAS and native Env, side and bottom views). The width of the IAS Env (90 Å) was slightly reduced as compared with the native Env, but the height remained the same (90 Å). The general features of the cryo-EM reconstructions of the native and the IAS Env were confirmed by reconstructions made using samples that had been negatively stained with uranyl acetate (Figure 4). The main difference was that the cavity did not extend as deeply as in the cryo-EM reconstructions. A likely reason was that the stain did not penetrate efficiently into this part of the Env. Also, the negatively stained Env was slightly lower than the vitrified Env. The resolution of the negative stain EM reconstructions was estimated to be 22 Å. Results from the final round of EMAN refinements of the native and IAS structure using vitrified specimens are shown in Figure 5. This includes some selected class averages and projections of the final 3D map for corresponding views of native and IAS Env (Figure 5A–D). One can discriminate increased density at the centre of the Env tip in the native form as compared with

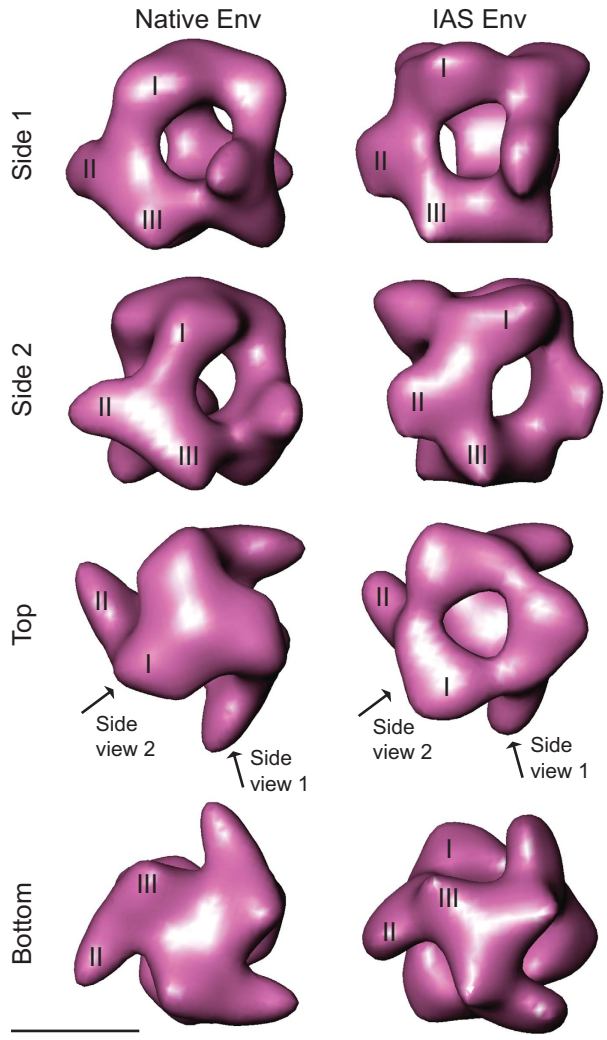

Figure 3 Surface-rendered 3D reconstructions of native and IAS Env using vitrified samples. EM images of native and IAS Env were subjected to image processing for reconstructing the native and the IAS Env trimer. Two side views, one top and one bottom view of native and IAS Env are shown. The projections of the side views are indicated in the top views. The top, middle and the lower projections are indicated by I, II and III, respectively. The isosurface has been set to enclose 100% of the expected volume of the complex. Scale bar represents 5 nm.

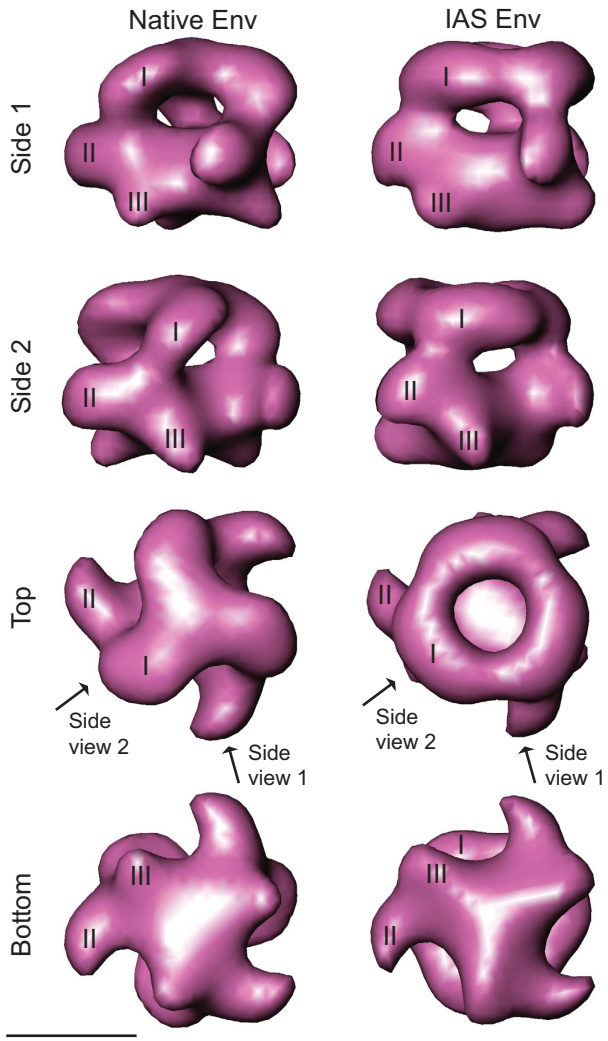

Figure 4 Surface-rendered 3D reconstructions of negatively stained native and IAS Env. EM images of uranyl acetate stained native and IAS Env were subjected to image processing. The 3D reconstructions are presented as described in Figure 3.

the IAS form (indicated by an arrow). Complete galleries of the class averages and map projections of all reconstructions are shown in Supplementary Figure 1.

RBD fitting

The RBD of F-MLV has been solved at 2-Å resolution (Fass *et al*, 1997). It is an L-shaped molecule and consists of an antiparallel β-sandwich and a helical subdomain. Because the Mo- and F-RBD have 89% amino-acid sequence identity and 97% conservation, we used the atomic structure of F-RBD to model the corresponding Mo-RBD structure (Zavorotinskaya and Albritton, 1999). Not surprisingly, the structure of the Mo-RBD looked almost identical to that of F-RBD. For convenience, we have described the Mo-RBD molecule as a head with a neck. The helical subdomain forms the front of the head and the β-sandwich the neck and the back of the head (Figure 6). We found that the Mo-RBD structure fitted well into the density of the upper protrusion of the protomer in the cryo-EM reconstruction of native Env (Figure 7, native Env, side views). In the Env trimer, the head-front of the RBD was directed towards the three-fold axis and the head-back and the neck towards the periphery (Figure 7, native Env, top view). The base of the neck associated with the upper part of the middle protrusion, possibly representing the C-terminal domain of SU. The RBD was tilted at its base backwards, lifting up the head-front at the three-fold axis, and towards its right side (Figure 7, native Env, side views). In the trimer, the head-fronts were not directly pointing towards each other but the heads intercalated so that the head-front of one RBD monomer approached the right side of the head-front in a neighbour monomer (Figure 7, native Env, top view). In an alternative fitting, the head-front of one RBD approached the left side of the head-front of the neighbour instead. However, this fitted the density map of native Env worse than the first alternative. In particular, rendering of the structure at high stringency ($\sigma = 3$) showed a good correlation between the map densities and the helical elements in the head-front of the RBD in the preferred location (data not shown).

In this location, most of the Mo-RBD surface was exposed to the solvent. The F-RBD has two complex sugar units, the

first residues of which were indicated in the crystal structure. The F-RBD units correspond to sugar units at Asn12 and Asn166 in Mo-RBD (indicated by sticks in Figure 6) (Felkner and Roth, 1992). The former unit is exposed on the upper-front part of the neck, projecting into the cavity of the trimer, and the latter on the left side of the neck, close to the base, projecting peripherally from the oligomer (Figure 7, native Env, side views). Two receptor-binding regions have been mapped on the Mo-RBD SU (Yoshimoto *et al*, 1993; MacKrell *et al*, 1996; Bae *et al*, 1997; Davey *et al*, 1997, 1999; Zavorotinskaya and Albritton, 1999). One (involving residues Arg83 and Asp84) was localized in the upper-front and the other (involving Trp142) in the upper-back part of the head (indicated by spheres in Figure 6). In our trimer model, the front receptor-binding site was exposed at the upper surface of the Env tip and the back site at its upper periphery (Figure 7, native Env, top and side views). Taken together, the front sites formed a triangle around the centre of the upper surface of the Env tip. The fitting of the RBD to the upper protrusion was unique so far as it was the only position, which allowed the exposure of both receptor-binding sites to the external surface of the trimer. Thus, if the RBD was fitted with the front receptor-binding site in the middle or in the lower protrusion, this resulted in the hiding of the back site in the interior of the trimer (data not shown). Therefore, we conclude that the upper protrusions of the native reconstruction represent the RBD of the Env. This also defines the membrane distal and proximal parts of the Env trimer.

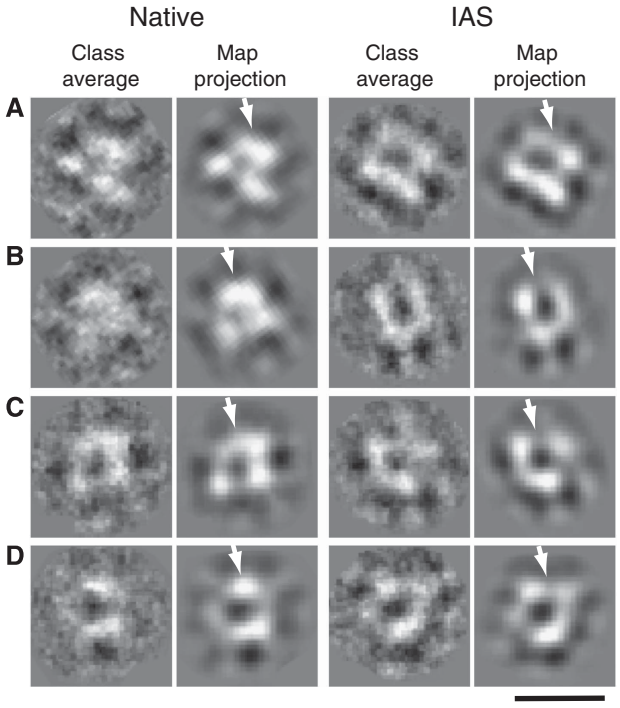

Figure 5 Refinement of native and IAS Env structure in vitrified samples. Some selected class averages and projections of the final 3D map for corresponding side views of native and IAS Env are shown (**A**–**D** in both panels). Class averages are displayed to the left and map projections to the right. Arrows in map projections indicate a density shift at the centre of the Env tip that accompanies the transition from native to IAS Env. Scale bar represents 10 nm.

The Mo-RBD also fits well into the upper protrusion of the cryo-EM reconstruction of the IAS Env (Figure 7, IAS Env, side and top views). Thus, during activation, the RBDs had turned out from their head-fronts-towards-centre position clockwise to the periphery, forming a triangular structure where the head-front of one RBD was positioned behind the head-back of a neighbour RBD. This turning is most clearly demonstrated when comparing the positions of a single RBD monomer in top view of native and IAS Envs (Figure 7, bottom left and bottom middle panels). Furthermore, the fitting of the RBD into IAS Env suggested that the RBDs did not interact with each other. The RBDs appeared to stand straight as an upside down L on the rest of IAS Env molecule, and not tilted as in native Env. Alternative fittings of the RBD with the front receptor-binding site in the middle or in the lower protrusion were restricted, not only by the hiding of the back receptor-binding site but also by the reduced size of the middle protrusion (data not shown).

Using the lower protrusions as reference points, we overlaid the electron density maps of the native and IAS Env (Figure 7, right panels). This confirmed the activation-mediated relocation of the RBD, shortening of the middle projection and thickening of the cavity floor. Furthermore, the superimposition indicated that the connection point of the RBD neck with the rest of the molecule was shifted clockwise in the IAS trimer relative to the native trimer. This was evident when comparing the overlaid native and IAS Env SU meshes in a transverse section of the trimer in the RBD neck region (Figure 7, bottom right panel). The position of the section is indicated by arrows in side view 2 of the overlaid meshes.

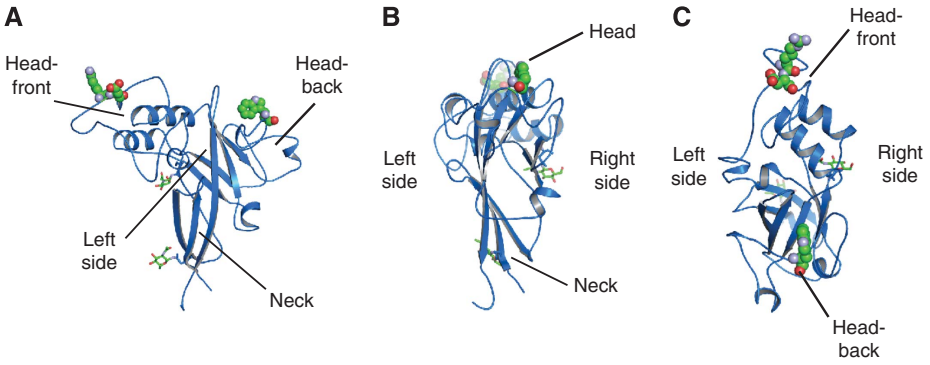

Figure 6 Structure of Mo-RBD. This was modelled using the crystal structure of F-RBD. Cartoon representations of the Mo-RBD structure from the side (**A**), back (**B**) and top (**C**) are shown. Residues in the two receptor-binding sites (front site: Arg83 and Asp84; back site: Trp142) are shown as spheres and the first residue of the two sugar units as sticks. The head, neck, right and left sides of RBD are indicated.

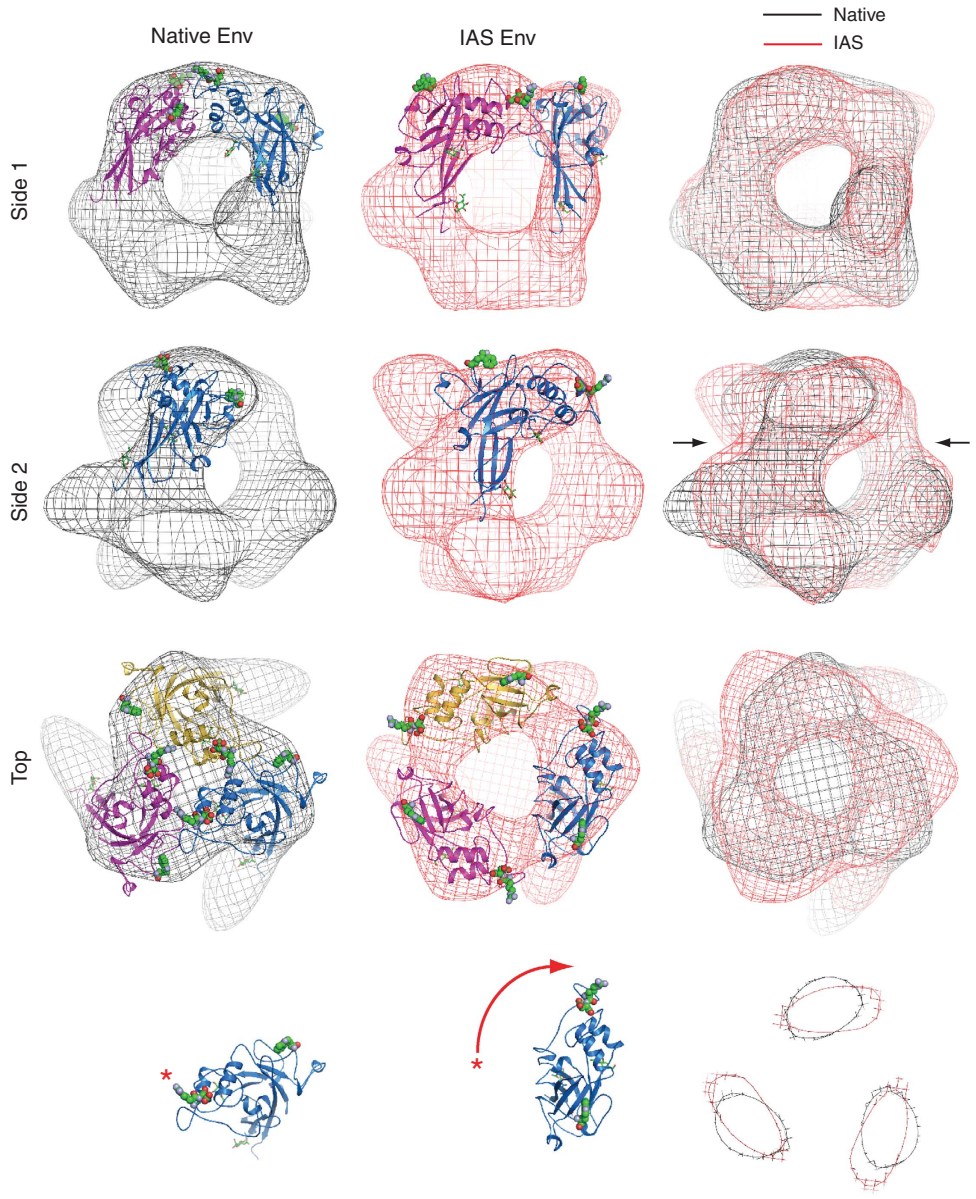

Figure 7 Left and middle panels: RBD fitting into the density maps of native (black surface mesh) and IAS Env (red mesh), reconstructed using vitrified samples. The atomic structure of the modelled Mo-RBD was manually fitted into the upper protrusions. Side view 1 displays two, side view 2 one and the top view three RBD monomers. The bottom left and bottom middle panels show a single RBD monomer (blue) in top view of native and IAS Env with surface mesh hidden to demonstrate the outward turning during activation. The head-front of RBD in native Env is indicated by an asterisk and the turning is indicated by an arrow. Right panels: superimposition of native and IAS Env density maps. The bottom right panel shows a transverse section through the lower neck region of the superimposed surface meshes of native (black) and IAS (red) Env. The position of the section in Env is indicated by two arrows in side view 2 of the superimposed density maps.

Discussion

A major assumption in this study was that the IAS Env obtained by Ca^{2+} depletion in the presence of alkylator corresponds to a structural intermediate in the receptor-activated Env. Its validity was suggested by several facts. First, Ca^{2+} depletion facilitates receptor-mediated fusion of virus with cells, whereas the reaction is reversibly suppressed by high Ca^{2+} (>1.8 mM) (Wallin *et al*, 2004). This suggests that removal of Ca^{2+} mediates receptor-induced activation as well. Second, receptor activation elicits a pathway of conformational changes that appears identical with that obtained *in vitro* by Ca^{2+} depletion. This includes a stage with the exposure of the CXXC thiol and the intersubunit disulphide for external modifications (IAS), the disulphide isomerization reaction and SU dissociation (Wallin *et al*, 2004; M Sjöberg, unpublished results). Finally, recent analyses by us have shown that Env triggering *in vitro* or *in vivo* results in a similarly SDS-sensitive IAS oligomer in the presence of alkylator and in an equally SDS-resistant activated TM trimer in the absence of alkylator (Sjöberg *et al*, 2008).

The reconstructions of the native and IAS Env from the EM images by image processing showed that the protomeric unit formed three protrusions. In the trimer, the units enclosed a large central cavity. The protrusion at one end of the protomer had the shape of a bent finger. In native Env, the tips of the bent fingers were directed against each other, closing the cavity from above, whereas in IAS Env they appeared rotated

sideways leaving the cavity open from above. The reliability of our EM reconstructions was strengthened by the fact that two different methods, vitrification and negative staining with uranyl acetate, for sample preparation yielded very similar results. In general, conformational changes induced by negative stain have been of great concern. Therefore, it is notable that this was not the case in our study. It is likely that artefacts were avoided because of rapid uranyl acetate-induced sample fixation as suggested by Zhao and Craig (2003).

A model for the atomic structure of the Mo-RBD was created based on the crystal structure of the highly homologous F-RBD (Fass *et al*, 1997). A good fit was found for the modelled Mo-RBD structure in the upper protrusions that limited the cavity of the native Env and in the corresponding protrusions of the opened IAS Env. This suggested that the initial stage of Env activation involves a major rotation of the RBD, possibly along the neck axis, a movement that opens the Env cavity from above. Furthermore, comparison of the native and IAS Env electron density maps showed that the attachment site of the neck on the upper part of the middle protrusion shifted its position in a clockwise direction. The fact that the RBD atomic model could be fitted into the upper protrusions also after the Env had undergone the conformational transition into the IAS form supports the correctness of the fit.

The two receptor-binding regions that have been mapped in the RBD are exposed in the native Env trimer, the upper-front sites around the three-fold axis in the centre of the Env tip and the upper-back sites at the periphery of the tip (Yoshimoto *et al*, 1993; MacKrell *et al*, 1996; Bae *et al*, 1997; Davey *et al*, 1997, 1999; Zavorotinskaya and Albritton, 1999). The latter sites appear to be more easily accessible, at least for multiple receptors. One RBD-binding site in the MCAT-1 receptor for MLV, a basic amino-acid transporter that spans the membrane multiple times, has been mapped to a region of the third extracellular domain (Albritton *et al*, 1989, 1993; Wang *et al*, 1991; Qian *et al*, 2003). Interestingly, the site does not seem to provide the full binding capacity of the receptor but an additional site might exist (Albritton *et al*, 1993; Qian *et al*, 2003). Therefore, it is possible that the MLV Env is opened up for fusion activation by the relocation of the RBDs in a two-step process: first, one site reacts with the peripheral-binding site in the RBD and then another one with the central site.

The location of the stabilizing Ca^{2+} ion(s) in the native structure is not known but it is tempting to suggest that they are coordinated by amino-acid side chains in the front part of the RBD heads. The initial receptor-binding event might disturb the coordination resulting in Ca^{2+} release and subsequent rotational movement of all RBDs into the open conformation.

Two alternative models for the organization of the RBD monomers in the Env trimer have been presented. These models were made without any structural data on the trimer. In one model, the RBDs were arranged with the backs of the heads interacting with each other at the three-fold axis, that is, in the opposite orientation as in our model of native Env (Fass, 1997). In the other model, the RBDs were arranged similar to the organization in our IAS Env, although without gaps between the monomers (Zavorotinskaya and Albritton, 1999). The interesting feature with the latter model was that it colocalized the front receptor-binding site of one monomer with the back site of another one. It was suggested that in this way one RBD-binding site of the receptor could interact with both receptor-binding sites on the RBD. Clearly, this organization is not found in the native Env, but it is still possible that the receptor-binding process involves the binding of the front and back sites of two different RBDs. This could stabilize the open structure of the RBDs in the IAS Env. However, binding *in vitro* of purified receptor and F-RBD in CHAPS indicated 1:1 binding (Davey *et al*, 1997).

Recently, a reconstruction of the Env complex in the Mo-MLV particle was made by cryo-EM tomography (Forster *et al*, 2005). This showed a roughly 10 nm × 10 nm trimeric particle composed of a head with multiple protrusions and three legs, which splayed outward towards the membrane, thus enclosing a membrane proximal cavity at the three-fold axis. Following one protomer out from the membrane to the top of the head, one could distinguish that the leg was made of two rod-like units possibly bent into each other at the head interphase. The head part contained two lower and two upper protrusions. It was proposed that the TM formed the leg as an 'inversed' hairpin and that, different from the general model for class I fusion protein activation, TM coil interactions at the three-fold axis would occur first after activation initiation. The RBD was suggested to be accommodated in the lower part of the head, lying on its right side with the front part of the head in the larger protrusion. The positioning of the large protrusion and the leg in the protomer shows some similarities with that of the middle and lower protrusions of our reconstruction. However, we cannot distinguish detailed features in the lower protrusion and the top part of the head portion appears quite different. Here, we find one L-shaped protrusion into which the RBD structure can be fitted very well.

The outward turning of the RBD head that accompanies the transition of the native Env of Mo-MLV into the IAS form could serve several purposes in activating Env for fusion. The RBDs in the IAS Env form together with the bound receptor(s) a well-like space between the rest of the Env molecule and the target cell membrane. This might, at a subsequent activation step, guide the formation of an extended (pre-hairpin) form of the TM subunits and the presentation of their fusion peptides to the target membrane. A somewhat similar structure has been found by cryo-EM of influenza A/Japan/305/57 haemagglutinin in low pH (4.9, 10 min at 4 °C)-activated particles, leading to similar conclusions (Bottcher *et al*, 1999). Recently, CD4-mediated activation of the HIV-1 glycoprotein was shown to involve a gp120–gp41 complex intermediate with gp41 exposing its fusion peptide in a pre-hairpin conformation (Chien *et al*, 2007).

The RBD well in the IAS Env could also function as an effective molecular sieve to restrict antibody access to the membrane fusion machinery putatively located within. If a similar structure is present in HTLV-1 and HIV-1, then this could explain the resistance to neutralizing antibodies targeting the coiled coil of the TM and gp41 pre-hairpin (Mirsaliotis *et al*, 2007).

Furthermore, it is reasonable to assume that the RBD turning generates the signal to the C-terminal part of the SU subunit that subsequently activates the TM for fusion. The RBD is linked to the C-terminal domain of SU through a 40-residue-long Pro-rich region (PRR). A similar segment protects the receptor-binding site in the gD protein in herpes

simplex virus 1, and transmits further fusion activation after displacement (Krummenacher *et al*, 2005). The gD is, similar to the RBD, folded as an immunoglobulin variable domain and the PRR is linked to its C-terminal end (Carfi *et al*, 2001). Therefore, it was suggested that the PRR of MLV might have a somewhat similar role (Rey, 2006). For instance, the PRR of MLV might prevent a fusion-activating interaction between the RBD and the SU-C-terminal domain and the receptor binding might release this inhibition. The model is supported by the phenotype of amphotropic 4070A MLV mutants with swapped PRR from Mo-MLV or F-MLV (Lavillette *et al*, 1998). These were found to be hyper-fusogenic, suggesting that the fusion inhibition of the heterologous PRR could very easily be relieved by the receptor. In view of our present results, the repositioning of the RBD on the upper part of the middle protrusion, that occurs when switching from the native to the IAS structure, could correspond to the establishment of the TM activating RBD–SU-C-terminal domain interaction.

Materials and methods

Cells and virus

Mo-MLV was grown in MOV-3 cells (G Schmidt, GSF-National Research Center for Environment and Health, Neuherberg, Germany). These were maintained in Dulbecco's modified Eagle's medium containing 4.5 g/l glucose (Gibco BRL) and supplemented with 10% FCS, 20 mM HEPES and L-glutamine. [^{35}S]Cys labelled wt Mo-MLV was prepared in MOV-3 cells by overnight labelling with 90 μCi/ml [^{35}S]Cys (GE Healthcare Biosciences, Buckinghamshire, UK) in the presence of 25 μM unlabelled cystein as described (Opstelten *et al*, 1998). Virus in supernatant was purified by sedimentation through a step-gradient composed of 3 ml 50% (w/w) and 7 ml 20% (w/w) sucrose in HN buffer (20 mM HEPES, 135 mM NaCl, pH 7.45) containing 1.8 mM $CaCl_2$. The gradient was run for 2 h at $RCF_{max} = 8.7 \times 10^4 g$ (22 k.r.p.m.) and 4 °C in a Beckman SW28 rotor. The virus-containing fractions were dialysed against HN buffer in Slide-A-Lyzer 3.5k dialysis cassettes (Pierce, Rockford, IL) and further concentrated on a step gradient composed of 16 μl 50% (w/w) and 32 μl 20% (w/w) sucrose in HN buffer, run for 1 h at $RCF_{max} = 8.7 \times 10^4 g$ (25 k.r.p.m.) and 4 °C in a Beckman TLS55 rotor.

Preparation and isolation of soluble native and IAS Env trimers

Native Env trimers were prepared by incubating Mo-MLV in HN buffer containing 1% Triton X-100 and 1.8 mM Ca^{2+} for 15 min on ice and residual sucrose was removed by gel filtration in a Zeba desalt spin column (Pierce). The trimers were purified by sedimentation in a 5–20% (w/w) sucrose gradient for 18 h at $RCF_{max} = 1.1 \times 10^5 g$ (32 k.r.p.m.) and 4 °C in a Beckman SW 55 rotor with adaptor number 356860. IAS Env trimers were prepared by incubating the virus in the solubilization buffer without Ca^{2+}, but with 10 mM EDTA and 10 mM NEM for 20 min at 37 °C, and isolated as described above.

Gel electrophoresis

Samples for BN–PAGE were mixed with an equal volume of 2 × BN sample buffer containing 100 mM morpholinepropanesulphonic acid (MOPS), 100 mM Tris–HCl, 40% glycerol, 0.1% Serva Blue G, pH 7.7 and incubated at room temperature for 10 min. Electrophoresis was carried out on 4.5–16% acrylamide (of which 2.6% comprised bis-acrylamide) gradient gels containing 50 mM Bis–Tris and 0.5 M 6-amino hexanoic acid, at 4 °C for 80 min at 200 V with 50 mM MOPS/50 mM Tris–HCl, pH 7.7, containing 0.002% Serva Blue G as cathode buffer and the same buffer without Serva Blue G as the anode buffer (Sattentau and Moore, 1991; Schagger and von Jagow, 1991). Non-reducing SDS–PAGE was carried out as described (Opstelten *et al*, 1998). The gels were dried and exposed to phosphorimage screens (BAS-MS2025; Fujifilm, Science Imaging Scandinavia, Nacka, Sweden) and the labelled proteins were visualized using a Molecular Imager FX and the *QuantityOne* program from Bio-Rad Laboratories (Hercules, CA). Non-radioactive viral proteins were stained by the nondiamin silver staining method (Merril, 1990).

Negative stain EM data collection

EM specimens were made using conventional negative staining of Env samples. In short, 4 μl of native or IAS Env trimers, which were more than 90% pure based on PAGE, was adsorbed to a glow-discharged carbon-coated grid. The sample was washed once with a drop of water, stained with a drop of 2% uranyl acetate and air dried. Images of the particles were recorded on Kodak S0163 film using a Philips CM120 transmission electron microscope at a magnification of × 45 000 and an acceleration voltage of 120 kV. Micrographs recorded at 1–2 μm under-focus were digitized with a Zeiss SCAI scanner using a step size of 21 μm corresponding to ∼4.7 Å per pixel on the specimen scale.

Cryo-EM data collection

Specimens (4 μl) were applied onto glow-discharged copper grids coated with a thin holey carbon film and subsequently plunge-frozen in liquid ethane using an FEI Vitrobot^{TM}. The data were recorded under low-dose conditions (∼10 e/Å^2 per exposure) in a JEOL2100F field emission gun transmission electron microscope with an accelerating voltage of 200 kV. The micrographs were recorded directly on a 4k × 4k CCD camera (Tietz Video and Image Processing Systems) with a 15 μm pixel size at a magnification of × 86 000 and at 2.5–8 μm under-focus. The pixel size was binned to 30 μm, which corresponds to ∼3.5 Å on the specimen scale. The high magnification was necessary for particle detection. The initial models were generated from the images at large under-focus (4–8 μm), which showed good contrast for particle extraction. The refined reconstructions were made using images with 2.5–3.5 μm under-focus.

Data processing

Manually picked particles were used for the generation of initial models (separate for each data set) with a C3 point group symmetry. These were used as reference for automatic extraction of images for the refined reconstructions. The images were corrected for contrast transfer function using *ctfit* in the EMAN software package. Standard iterative procedures in EMAN (version 1.7) were then used for refinement of the models in C3 point group symmetry (Ludtke *et al*, 1999). The refinement cycle was repeated until no further change was observed. An even distribution of particle orientations was included in the analyses (Supplementary Figure 2). The resolution was determined by Fourier shell correlation at the coefficient value of 0.5 using the EMAN program *eotest* (Supplementary Figure 3).

Molecular modeling

The atomic model for the Mo-RBD (accession number: P003385) was obtained using the atomic structure of the highly homologous F-RBD (Fass *et al*, 1997) (Protein Data Bank ID, 1AOL) and the SWISS-MODEL protein structure homology-modelling server (accessible through the ExPASy web server). Manual fitting of the modelled Mo-RBD into the density map of the native and IAS Env protomer was guided by overall fitting of the atomic model into the EM map, by the exposure of sugar units and receptor-binding regions of RBD on the SU and the upper periphery, respectively, of the Env trimer and by the steric constraints of the three-fold symmetry. All docking was done using the program O. The 3D visualization was done using Iris explorer and PyMOL.

Accession number

The electron density map has been deposited in the EMDB database (accession code EMD-2863 and EMD-2864).

Supplementary data

Supplementary data are available at *The EMBO Journal* Online (http://www.embojournal.org).

Acknowledgements

We are grateful to Lennart Nilsson and Lena Hammar for advice. Swedish science foundation grant 2778 and Swedish cancer foundation grant 0525 to HG supported this study.

References

Albritton LM, Kim JW, Tseng L, Cunningham JM (1993) Envelope-binding domain in the cationic amino acid transporter determines the host range of ecotropic murine retroviruses. *J Virol* **67:** 2091–2096

Albritton LM, Tseng L, Scadden D, Cunningham JM (1989) A putative murine ecotropic retrovirus receptor gene encodes a multiple membrane-spanning protein and confers susceptibility to virus infection. *Cell* **57:** 659–666

Bae Y, Kingsman SM, Kingsman AJ (1997) Functional dissection of the Moloney murine leukemia virus envelope protein gp70. *J Virol* **71:** 2092–2099

Barnett AL, Cunningham JM (2001) Receptor binding transforms the surface subunit of the mammalian C-type retrovirus envelope protein from an inhibitor to an activator of fusion. *J Virol* **75:** 9096–9105

Bottcher C, Ludwig K, Herrmann A, van Heel M, Stark H (1999) Structure of influenza haemagglutinin at neutral and at fusogenic pH by electron cryo-microscopy. *FEBS Lett* **463:** 255–259

Bullough PA, Hughson FM, Skehel JJ, Wiley DC (1994) Structure of influenza haemagglutinin at the pH of membrane fusion. *Nature* **371:** 37–43

Carfi A, Willis SH, Whitbeck JC, Krummenacher C, Cohen GH, Eisenberg RJ, Wiley DC (2001) Herpes simplex virus glycoprotein D bound to the human receptor HveA. *Mol Cell* **8:** 169–179

Chan DC, Fass D, Berger JM, Kim PS (1997) Core structure of gp41 from the HIV envelope glycoprotein. *Cell* **89:** 263–273

Chen B, Vogan EM, Gong H, Skehel JJ, Wiley DC, Harrison SC (2005) Structure of an unliganded simian immunodeficiency virus gp120 core. *Nature* **433:** 834–841

Chien MP, Jiang S, Chang DK (2007) The function of coreceptor as a basis for the kinetic dissection of HIV type 1 envelope protein-mediated cell fusion. *FASEB J* **21:** 21

Davey RA, Hamson CA, Healey JJ, Cunningham JM (1997) *In vitro* binding of purified murine ecotropic retrovirus envelope surface protein to its receptor, MCAT-1. *J Virol* **71:** 8096–8102

Davey RA, Zuo Y, Cunningham JM (1999) Identification of a receptor-binding pocket on the envelope protein of friend murine leukemia virus. *J Virol* **73:** 3758–3763

Fass D (1997) The protein structures underlying receptor binding and membrane fusion of ecotropic murine leukemia virus. Vol. Ph D thesis, Department of Biology, Massachusetts Institute of Technology, Cambridge, p 142

Fass D, Davey RA, Hamson CA, Kim PS, Cunningham JM, Berger JM (1997) Structure of a murine leukemia virus receptor-binding glycoprotein at 2.0 angstrom resolution. *Science* **277:** 1662–1666

Fass D, Harrison SC, Kim PS (1996) Retrovirus envelope domain at 1.7 angstrom resolution. *Nat Struct Biol* **3:** 465–469

Felkner RH, Roth MJ (1992) Mutational analysis of the N-linked glycosylation sites of the SU envelope protein of Moloney murine leukemia virus. *J Virol* **66:** 4258–4264

Forster F, Medalia O, Zauberman N, Baumeister W, Fass D (2005) Retrovirus envelope protein complex structure *in situ* studied by cryo-electron tomography. *Proc Natl Acad Sci USA* **102:** 4729–4734

Huang CC, Tang M, Zhang MY, Majeed S, Montabana E, Stanfield RL, Dimitrov DS, Korber B, Sodroski J, Wilson IA, Wyatt R, Kwong PD (2005) Structure of a V3-containing HIV-1 gp120 core. *Science* **310:** 1025–1028

Hunter E (1997) Viral entry and receptors. In *Retroviruses*, Coffin JM, Hughes SH, Varmus HE (eds), pp 71–119. NY: Cold Spring Harbor Laboratory Press

Kayman SC, Park H, Saxon M, Pinter A (1999) The hypervariable domain of the murine leukemia virus surface protein tolerates large insertions and deletions, enabling development of a retroviral particle display system. *J Virol* **73:** 1802–1808

Kobe B, Center RJ, Kemp BE, Poumbourios P (1999) Crystal structure of human T cell leukemia virus type 1 gp21 ectodomain crystallized as a maltose-binding protein chimera reveals structural evolution of retroviral transmembrane proteins. *Proc Natl Acad Sci USA* **96:** 4319–4324

Krummenacher C, Supekar VM, Whitbeck JC, Lazear E, Connolly SA, Eisenberg RJ, Cohen GH, Wiley DC, Carfi A (2005) Structure of unliganded HSV gD reveals a mechanism for receptor-mediated activation of virus entry. *EMBO J* **24:** 4144–4153

Kumar P, Nachagari D, Fields C, Franks J, Albritton LM (2007) Host cell cathepsins potentiate Moloney murine leukemia virus infection. *J Virol* **81:** 10506–10514

Kwong PD, Wyatt R, Robinson J, Sweet RW, Sodroski J, Hendrickson WA (1998) Structure of an HIV gp120 envelope glycoprotein in complex with the CD4 receptor and a neutralizing human antibody. *Nature* **393:** 648–659

Lavillette D, Boson B, Russell SJ, Cosset FL (2001) Activation of membrane fusion by murine leukemia viruses is controlled in cis or in trans by interactions between the receptor-binding domain and a conserved disulfide loop of the carboxy terminus of the surface glycoprotein. *J Virol* **75:** 3685–3695

Lavillette D, Maurice M, Roche C, Russell SJ, Sitbon M, Cosset FL (1998) A proline-rich motif downstream of the receptor binding domain modulates conformation and fusogenicity of murine retroviral envelopes. *J Virol* **72:** 9955–9965

Ludtke SJ, Baldwin PR, Chiu W (1999) EMAN: semiautomated software for high-resolution single-particle reconstructions. *J Struct Biol* **128:** 82–97

MacKrell AJ, Soong NW, Curtis CM, Anderson WF (1996) Identification of a subdomain in the Moloney murine leukemia virus envelope protein involved in receptor binding. *J Virol* **70:** 1768–1774

Merril CR (1990) Gel-staining techniques. *Methods Enzymol* **182:** 477–488

Mirsaliotis A, Nurkiyanova K, Lamb D, Kuo CW, Brighty DW (2007) Resistance to neutralization by antibodies targeting the coiled coil of fusion-active envelope is a common feature of retroviruses. *J Biol Chem* **282:** 36724–36735

Opstelten DJ, Wallin M, Garoff H (1998) Moloney murine leukemia virus envelope protein subunits, gp70 and Pr15E, form a stable disulfide-linked complex. *J Virol* **72:** 6537–6545

Pinter A, Honnen WJ, Tung JS, O'Donnell PV, Hammerling U (1982) Structural domains of endogenous murine leukemia virus gp70s containing specific antigenic determinants defined by monoclonal antibodies. *Virology* **116:** 499–516

Pinter A, Kopelman R, Li Z, Kayman SC, Sanders DA (1997) Localization of the labile disulfide bond between SU and TM of the murine leukemia virus envelope protein complex to a highly conserved CWLC motif in SU that resembles the active-site sequence of thiol-disulfide exchange enzymes. *J Virol* **71:** 8073–8077

Qian Z, Donald R, Wang H, Chen Q, Albritton LM (2003) Identification of a critical basic residue on the ecotropic murine leukemia virus receptor. *J Virol* **77:** 8596–8601

Rey FA (2006) Molecular gymnastics at the herpesvirus surface. *EMBO Rep* **7:** 1000–1005

Sattentau QJ, Moore JP (1991) Conformational changes induced in the human immunodeficiency virus envelope glycoprotein by soluble CD4 binding. *J Exp Med* **174:** 407–415

Schägger H, von Jagow G (1991) Blue native electrophoresis for isolation of membrane protein complexes in enzymatically active form. *Anal Biochem* **199:** 223–231

Sjöberg M, Lindqvist B, Garoff H (2008) Stabilization of TM trimer interactions during activation of Moloney murine leukemia virus Env. *J Virol* **82:** 2358–2366

Skehel JJ, Wiley DC (2000) Receptor binding and membrane fusion in virus entry: the influenza hemagglutinin. *Annu Rev Biochem* **69:** 531–569

Wallin M, Ekström M, Garoff H (2004) Isomerization of the intersubunit disulphide-bond in Env controls retrovirus fusion. *EMBO J* **23:** 54–65

Wallin M, Ekström M, Garoff H (2005a) The fusion-controlling disulfide bond isomerase in retrovirus env is triggered by protein destabilization. *J Virol* **79:** 1678–1685

Wallin M, Ekström M, Garoff H (2006) Receptor triggered but alkylation-arrested Env of murine leukaemia virus reveals the transmembrane subunit in a prehairpin conformation. *J Virol* **80:** 9921–9925

Wallin M, Löving R, Ekström M, Li K, Garoff H (2005b) Kinetic analyses of the surface-transmembrane disulfide bond isomerization-controlled fusion activation pathway in Moloney murine leukemia virus. *J Virol* **79:** 13856–13864

Wang H, Kavanaugh MP, North RA, Kabat D (1991) Cell-surface receptor for ecotropic murine retroviruses is a basic amino-acid transporter. *Nature* **352:** 729–731

Weissenhorn W, Dessen A, Harrison SC, Skehel JJ, Wiley DC (1997) Atomic structure of the ectodomain from HIV-1 gp41. *Nature* **387:** 426–430

Wilson IA, Skehel JJ, Wiley DC (1981) Structure of the haemagglutinin membrane glycoprotein of influenza virus at 3 Å resolution. *Nature* **289:** 366–373

Yoshimoto T, Yoshimoto E, Meruelo D (1993) Identification of amino acid residues critical for infection with ecotropic murine leukemia retrovirus. *J Virol* **67:** 1310–1314

Zavorotinskaya T, Albritton LM (1999) A hydrophobic patch in ecotropic murine leukemia virus envelope protein is the putative binding site for a critical tyrosine residue on the cellular receptor. *J Virol* **73:** 10164–10172

Zhao FQ, Craig R (2003) Capturing time-resolved changes in molecular structure by negative staining. *J Struct Biol* **141:** 43–52

